Environ. Sci. Technol. 1995, 29, 1446–1455

Wettability Effects on Scaling Two- and Three-Fluid Capillary Pressure—Saturation Relations

SCOTT A. BRADFORD AND FEIKE J. LEIJ*

U.S. Salinity Laboratory, U.S. Department of Agriculture, Agricultural Research Service, 450 Big Springs Road, Riverside, California 92507

Capillary pressure (P_c) - saturation (S) relationships for porous media containing three fluids are often predicted from two-fluid P_c-S curves. This practice was investigated for porous media with different wettabilities. Two- and three-fluid P_c-S curves were measured, using an automated setup, for sands containing air and water; air and oil, oil and water, and air, oil, and water. Similar P_c-S curves were found for air–oil systems while differences occurred for air–water or oil–water due to differences in hydrophobicity and contact angle hysteresis. Three-fluid P_c-S curves could be accurately predicted for hydrophilic media from two-fluid P_c-S data with scaling, using fitted contact angles and measured interfacial tensions, and Leverett's assumption. Such predictions were found to be inadequate for hydrophobic media because the intermediate fluid is presumably discontinuous.

Introduction

Deterministic multiphase flow models have been developed to predict the spatial and temporal distribution of immiscible organic compounds in the subsurface environment. Compared to the advances in numerical modeling of multiphase flow problems, little progress has been made in quantifying the P_c-S relations required by these models (*1*). The capillary pressure is typically described in an empirical way as a function of fluid saturation; the fluid distribution depends on other factors such as surface tension, wettability of the solid, fluid viscosity, grain size distribution, and solution chemistry (*2*).

Scaling P_c-S data for a particular two-fluid system is commonly used to predict P_c-S curves for other fluid pairs in the same medium (*3*). Since the measurement of three-fluid P_c-S relations is significantly more cumbersome than that of two-fluid P_c-S curves; three-fluid P_c-S functions are often predicted from two-fluid data as first proposed by Leverett (*4*). The prediction of P_c-S curves for air–oil–water systems is based on the limiting assumptions that the medium (solid) is strongly wetted by one fluid (e.g., water) and that the intermediate wetting fluid (e.g., an organic liquid) forms a continuous layer between the wetting and nonwetting (e.g., air) fluids. Lenhard and Parker (*5*) were the first to verify Leverett's assumption on strongly water-wet sands with a spreading organic liquid.

The wettability of a solid refers to the tendency of one fluid to spread on or adhere to the solid surface in the presence of other immiscible fluids. Since the fluid distribution is influenced by the solid's wettability, wettability should be considered before applying Leverett's assumption and scaling procedures. Treiber et al. (*6*) measured contact angles for 55 oil reservoirs and found that 37 were oil-wet. Anderson (*7*) reported that coal, graphite, sulfur, talc, talc-like silicates, and many sulfides are probably neutrally wet to oil-wet. On the other hand, common aquifer materials, such as quartz, carbonates, and sulfates, are strongly water-wet. Wetting can be altered by physical, chemical, or biological means (*8*). Demond et al. (*9*) and Powers and Tambin (*10*) recently reported that cationic surfactants and additives to gas can cause water-wet materials to become oil-wet. Results presented by Ebsch and Gierke (*11*) and Stallard et al. (*12*) indicate that some clays may be oil-wet. These findings suggest that porous media are not necessarily strongly water-wet.

In view of the above, the objectives of this paper are to (i) observe the effects of various wetting conditions on two- and three-fluid P_c-S relations and (ii) analyze the applicability of Leverett's assumption and related multiphase scaling approaches.

Theory

Wettability. At equilibrium, fluids are distributed to the state with the lowest possible energy content as determined by the wettability of the porous medium. The wettability of a solid surface is characterized by the contact angle (ϕ), which is determined by a horizontal force balance when a lighter fluid (l), denser fluid (d), and a flat solid surface (s)

* Corresponding author e-mail address: titan@ucracl.ucr.edu; Fax: (909) 369-4818.

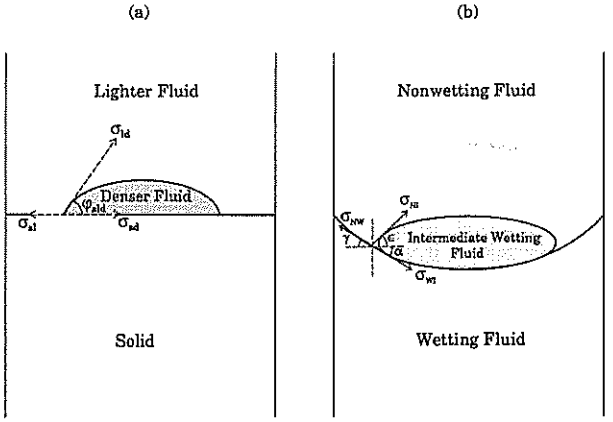

FIGURE 1. Hypothetical distribution of fluids and interfacial tensions at (a) a solid–lighter fluid–denser fluid contact line and (b) a wetting–intermediate–nonwetting fluid contact line.

meet at a three-phase contact line, as shown in Figure 1a. According to Young's equation

$$\cos(\phi_{sld}) = (\sigma_{sl} - \sigma_{sd})/\sigma_{ld} \quad (1)$$

where σ is the interfacial tension (N/m) and the subscripts indicate the phases. The denser fluid wets the solid surface for $\phi_{sld} < 90°$ while the lighter fluid wets the solid surface for $\phi_{sld} > 90°$. The fluid that does not wet the solid is known as the nonwetting fluid (*N*). Different contact angles may occur when the wetting fluid (*W*) is advancing (ϕ_{sld}^{A}) or receding (ϕ_{sld}^{R}). The equilibrium contact angle, ϕ_{sld}, corresponds to a unique free energy minimum; ϕ_{sld}^{A} and ϕ_{sld}^{R} differ from ϕ_{sld} during metastable states (*13*).

In a system with two liquids, either water (w) or oil (o) wets the solid; the other liquid is the nonwetting fluid in a two-fluid system or the intermediate wetting fluid (I) in a three-fluid system. If present, air (a) is always the nonwetting fluid. Figure 1b illustrates that the wettability at the contact line of all three fluids is related to the coefficient of spreading, $\Sigma_{I/W}$, for a drop of an intermediate fluid on a wetting fluid defined as

$$\Sigma_{I/W} = \sigma_{NW} - (\sigma_{NI} + \sigma_{IW}) \quad (2)$$

The spreading coefficient can be viewed as the difference in adhesion (of the intermediate and wetting fluids) and cohesion (of the intermediate fluid). The tendency of the intermediate fluid to spread on the wetting fluid is proportional to $\Sigma_{I/W}$; a negative value for $\Sigma_{I/W}$ indicates that the intermediate fluid does not spread on the wetting fluid while a positive value indicates a tendency for spreading of the intermediate fluid. If an oil drop spreads on water, a water drop will not do so on this oil.

Capillarity. Figure 2 illustrates the equilibrium fluid distributions when capillary tubes preferentially wetted by a denser fluid and a lighter fluid are placed in a two-fluid system. The difference in pressure between the nonwetting and wetting fluids, i.e., the pressure drop over the curved interface, determines the capillary pressure. Laplace's equation defines the equilibrium capillary pressure as

$$P_c = P_N - P_W = \frac{2\sigma_{NW}}{R}\cos(\phi_{sNW}) \quad (3)$$

where R is the radius of the capillary tube. Note that $P_c = P_{ow} = P_o - P_w$ for a water-wet system, while $P_c = P_{ow} = P_w - P_o$ for an oil-wet system. A negative P_c implies a wetting

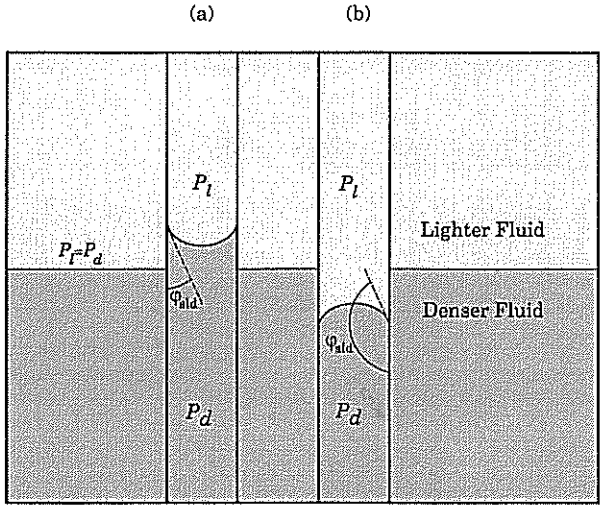

FIGURE 2. Hypothetical equilibrium fluid distributions and contact angles in capillary tubes wetted by (a) a denser fluid and (b) a lighter fluid after being immersed into a two-fluid system.

reversal and P_c should actually be redefined (*14*). For air–water or air–oil systems, the nonwetting fluid (air) is usually ignored since the liquid pressure is taken with respect to atmospheric pressure.

Scaling has been proposed as a way of obtaining P_c–S relations for a fluid system if P_c–S data are available for another fluid pair for the same porous medium. It follows from eq 3 that for the same porous medium the capillary pressure for one two-fluid system (subscript 1) can be predicted from another two-fluid system (subscript 2) according to

$$P_{c1}(S) = \frac{\sigma_1 \cos(\phi_1^{A,R})}{\sigma_2 \cos(\phi_2^{A,R})} P_{c2}(S) \quad (4)$$

where $\phi^{A,R}$ denotes an advancing or receding contact angle. A common scaling approach is based on the ratio of interfacial tensions of the fluid pairs when $\phi_1 = \phi_2$ in eq 4. Amyx et al. (*15*) observed that the $P_c - S$ drainage curves were scaled reasonably well with the ratio of interfacial tension alone for $\phi_{sld} < 50°$. Various relationships have been used, with limited success, to scale $P_c - S$ curves at different wettabilities by including contact angles (*3, 7, 16, 17*). The application of scaling procedures requires accurate values for ϕ_{sld}, ϕ_{sld}^{A}, and ϕ_{sld}^{R}.

In a three-fluid system, if the intermediate fluid forms a continuous layer, a drop in capillary pressure occurs over the nonwetting–intermediate and intermediate–wetting interfaces. Leverett (*4*) suggested that the pressure drop over the two-fluid nonwetting–intermediate and intermediate–wetting interfaces could be used to predict the pressure drop over the corresponding interfaces in a three-fluid system when S_I^{NI} equals S_{tI}^{NIW} ($S_{tI}^{NIW} = S_W^{NIW} + S_I^{NIW}$) and S_W^{IW} equals S_W^{NIW}, respectively. Here S is used for the degree of saturation, expressed as volume of fluid per volume of pore space, pertaining to the intermediate fluid (subscript I) or wetting fluid (subscript W) in a two-fluid (superscript NW, NI, IW), or three-fluid (superscript NIW) system. Leverett's assumption can be stated as

$$P_{NI}(S_{tI}^{NIW}) = P_{NI}(S_I^{NI}) \quad (5)$$

$$P_{IW}(S_W^{NIW}) = P_{IW}(S_W^{IW}) \quad (6)$$

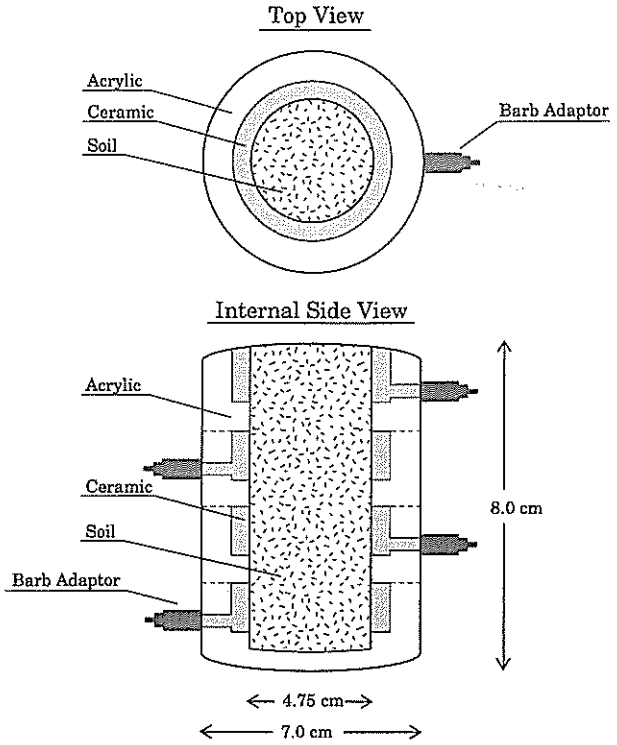

FIGURE 3. Schematic of soil column consisting of hydrophilic and hydrophobic ring tensiometers for independent control of water and oil phases, respectively.

Lenhard and Parker (*18*) used a scaling procedure, based upon eq 4 (assuming $\phi_1 = \phi_2$) and Leverett's assumption, for predicting the three-fluid system P_c–S curve from a two-fluid reference curve as follows:

$$P_{NW}(\overline{S_W^{NW}}) = \frac{\sigma_{NW}}{\sigma_{IW}} P_{IW}(\overline{S_W^{NIW}}) = \frac{\sigma_{NW}}{\sigma_{NI}} P_{NI}(\overline{S_{tI}^{NIW}}) \quad (7)$$

where the effective saturation $\bar{S}$ is given by $(S - S_r)/(1 - S_r)$ with S_r as the residual saturation.

Materials and Methods

The influence of wettability on two- and three-fluid systems was investigated by measuring two- and three-fluid P_c–S relations for a mixture of blasting sands treated with organosilane compounds to obtain different wetting characteristics. This section outlines the techniques to (i) determine the P_c–S relations and (ii) treat the blasting sands.

Two- and three-fluid P_c–S relations were obtained according to the "Brooks method" by displacing a known volume of fluid into or from the porous medium and measuring the (equilibrium) fluid pressures (*19*). Figure 3 shows a schematic of a column, which consists of hydrophilic and hydrophobic ring tensiometers. The design facilitates the fairly rapid measurement of P_c–S data; the two ring tensiometers for each liquid minimize hysteresis during internal redistribution while the (measured) fluid pressure represents a value at the center of the column. If the medium contains air, it is kept at atmospheric pressure by venting the column at the top.

P_c–S relationships were obtained with the setup shown in Figure 4, which is an automated version of the one employed by Lenhard and Parker (*5*). The data logger operates stepping motors and solenoid valves and monitors pressure transducer readings. The stepping motors are used to adjust vacuum–pressure regulators, which are connected to burets filled with water or oil through three-way solenoid valves. Two- and three-way solenoid valves were opened for 2 h at each measurement point to allow flow between the soil column and the buret so as to establish a new saturation level. The valves were then closed to achieve equilibrium fluid distributions in the medium. The oil and water pressures in the sample were monitored with ring tensiometers connected to a pressure transducer through a scanning valve. Fluid saturations in the sample were obtained from the buret readings, also monitored with a pressure transducer.

For all P_c–S measurements, a column of known volume was filled with the initial wetting fluid and packed with a predetermined mass of a blasting sand mixture to obtain a dry bulk density (ϱ_b) of 1.71 g/cm^3. The initial wetting fluid was oil for the air–oil systems and water for the air–water, oil–water, and air–oil–water systems. Soltrol 220, a mixture of C_{13}–C_{17} hydrocarbons with a fluid density, ϱ_o, of 0.8 g/cm^3, was used as oil (Phillips Petroleum Co., Bartlesville, OK 74004). The equilibrium fluid interfacial tensions, measured with a du Noüy ring (*20*), were σ_{aw} = 0.072 N/m, σ_{ao} = 0.024 N/m, and σ_{ow} = 0.026 N/m. The equilibrium value of the interfacial tension for the soltrol contaminated air–water interface, σ_{aw}^*, was 0.052 N/m. The porous medium was a mixture of several blasting sands containing 12.6% each of sizes 12 and 16, 25.2% each of sizes 20 and 30, and 8.2% each of sizes 60, 70, and 90 (Corona Industrial Sand Co., Corona, CA 91718). This distribution corresponds to 25% very coarse sand, 50% coarse–medium sand, and 25% fine sand according to the USDA textural classification (*21*). The porosity of the medium was calculated by assuming a specific density of 2.65 g/cm^3 (*22*). The initial volume of the wetting fluid was assumed to be equal to the product of column volume and porosity.

Primary drainage and main imbibition branches of the P_c–S curves were measured for all two-fluid systems. For three-fluid systems, oil was incrementally imbibed into a medium containing air and residual water to obtain an air–oil–water system. Various drainage and imbibition paths were followed to achieve a wide range of oil, water, and air contents.

To obtain different degrees of hydrophobicity, blasting sands were treated with organosilane compounds. The sands were added to a 5% solution of an organosilane (octadecyltrichlorosilane, OTS; vinyltriethoxysilane, VTS; or glycidoxypropyltrimethoxysilane, GPTS) in ethanol and mixed in a shaker for 5 h, after which the sands were air-dried (*23*). The organosilanes were selected on the basis of reported values for the solid–air interfacial tensions, σ_{sa}, of 0.0225 N/m for OTS, 0.025 N/m for VTS, and 0.0425 N/m for GPTS (*23*, *24*). Lower values for σ_{sa} reflect increasing hydrophobicity. An untreated sand was also used for P_c–S measurements; σ_{sa} is then assumed to be that of fused silica 0.078 N/m (*13*).

Results and Discussion

Two-Fluid Systems. In this section, the two-fluid P_c–S curves for air–water, air–oil, and oil–water systems obtained for treated and untreated sands will be discussed—particularly the effects of hydrophobicity. Note that all pressures are expressed in centimeters of water.

Figure 5 shows the P_{ao}–S_o^{ao} relations for drainage and imbibition of air–oil systems in four different sands. The P_{ao}–S_o^{ao} relations are similar for all treatments, indicating that the oil strongly wets the solid surfaces for all different

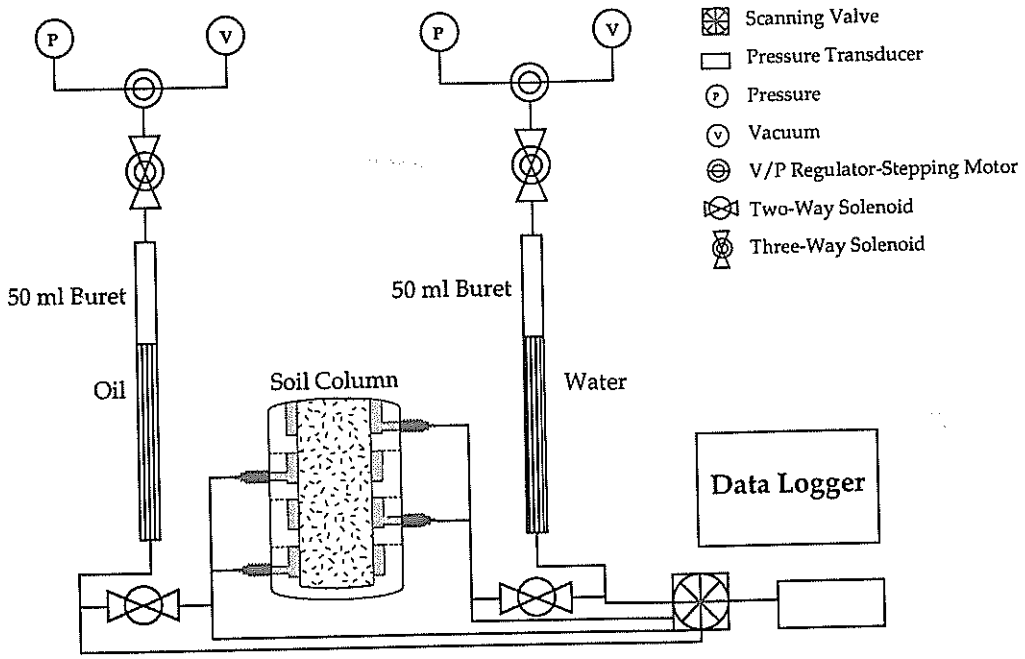

FIGURE 4. Sketch of setup for the automated measurement of P_c–S data.

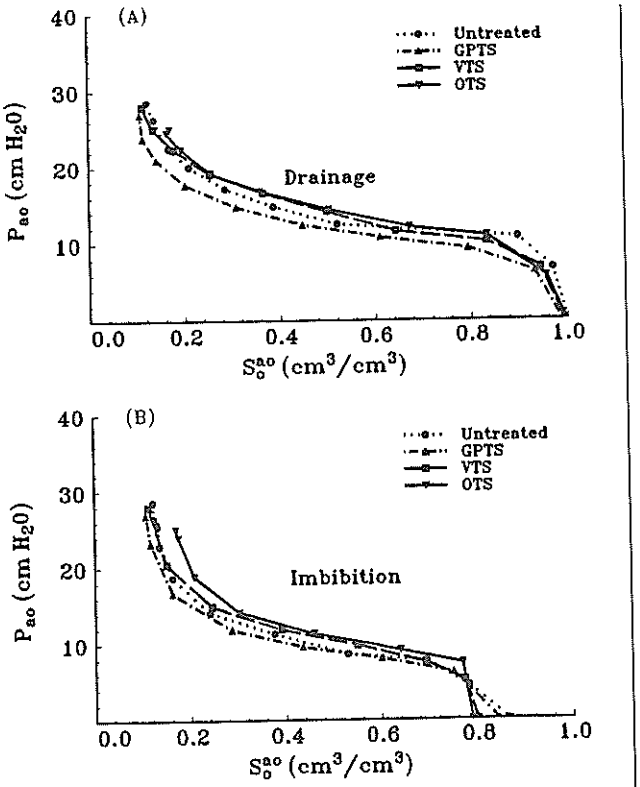

FIGURE 5. Measured (A) drainage and (B) imbibition P_{ao}–S_o^{ao} relations for air–oil systems.

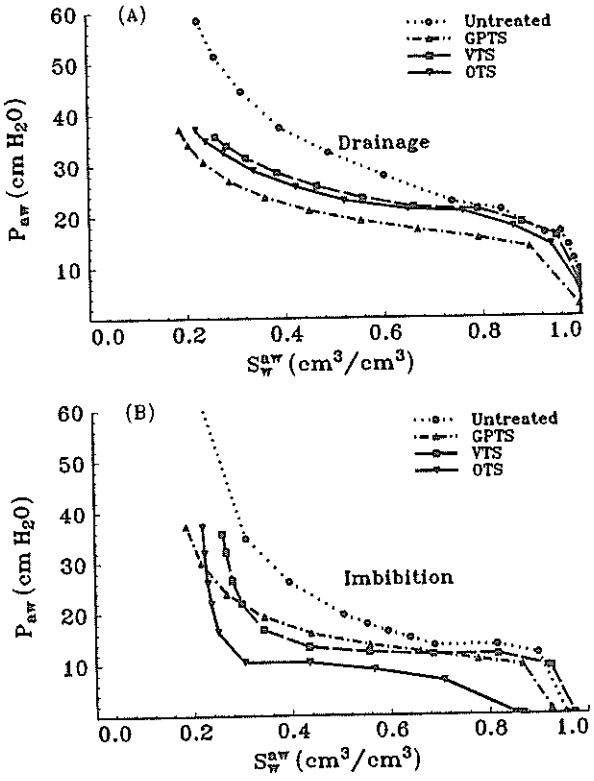

FIGURE 6. Observed (A) drainage and (B) imbibition P_{aw}–S_w^{aw} relations for air–water systems.

treatments. Contact angle hysteresis is negligible if oil spreads over the solid surface or if $\phi_{sao} = 0°$ and hysteresis in the P_{ao}–S_o^{ao} relation is primarily due to pore geometry and air entrapment.

Figure 6 shows the P_{aw}–S_w^{aw} relations for drainage and imbibition for air–water systems. Observe in Figure 6B that during imbibition P_{aw} decreases in the order untreated, GPTS, VTS, and OTS for a given S_w^{aw}. In contrast, Figure 6A shows that during drainage the GPTS treatment has the lowest P_{aw} for a given S_w^{aw}, whereas the other treatments follow the same sequence as in Figure 6B. A possible explanation is contact angle hysteresis (according to Laplace's equation, a higher ϕ_{saw} results in a lower capillary pressure). Morrow (*25*) compared values of ϕ_{sld}^{A} and ϕ_{sld}^{R} obtained for rough and smooth surfaces and found that contact hysteresis was dramatically less pronounced for smooth surfaces. The results of the P_{aw}–S_w^{aw} curves shown in Figure 6 suggest that the untreated, VTS, and OTS sands have rough surfaces and that the GPTS treatment may have resulted in a smooth surface. The fitted values of ϕ_{saw}^{A} and ϕ_{saw}^{R} shown in Table 1 also support this assumption; the method for determining ϕ will be discussed shortly.

TABLE 1

Fitted Advancing and Receding Contact Angles (deg) for Air–Water and Oil–Water Systems

	ϕ_{saw}^{A}	ϕ_{saw}^{R}	ϕ_{sow}^{A}	ϕ_{sow}^{R}
untreated	32.7	0.0	51.6	0.0
GPTS	46.6	48.2	64.7	66.8
VTS	52.2	35.6	103.3	45.9
OTS	64.8	37.6	146.0	62.1

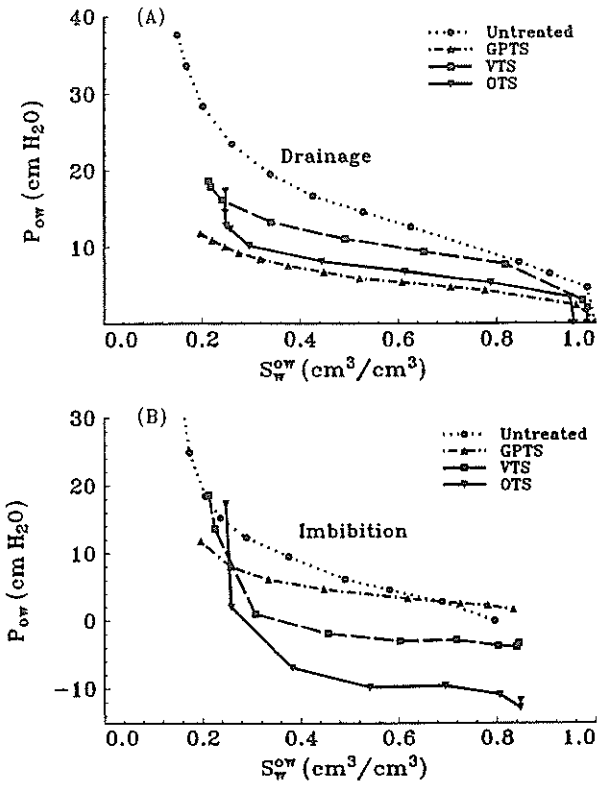

FIGURE 7. Observed (A) drainage and (B) imbibition P_{ow}–S_w^{ow} relations for oil–water systems.

The P_{ow}–S_w^{ow} relationships for drainage and imbibition in oil–water systems are illustrated in Figure 7. The P_{ow}–S_w^{ow} curves follow a trend similar to the P_{aw}–S_w^{aw} curves in Figure 6; the capillary pressure at a particular saturation has the same order during drainage (untreated > VTS > OTS > GPTS) and imbibition (untreated > GPTS > VTS > OTS). This result may also be explained by surface roughness (contact angle hysteresis). During drainage (Figure 7A) all values for $P_{ow} = P_o - P_w$ were found to be positive (water-wet), while Figure 7B (imbibition) shows that OTS and VTS sands had negative P_{ow} values for $S_w^{ow} > 0.28$ and $S_w^{ow} > 0.34$, respectively. Imbibing water beyond this saturation was only possible when oil was under suction relative to water ($P_o < P_w$). The OTS and VTS sands behaved as if they were water-wet during drainage and oil-wet during imbibition.

Several explanations are possible for the wetting reversal. One possible explanation is contact angle hysteresis. If $\phi_{sow}^{R} < 90°$ (hydrophilic solid) and $\phi_{sow}^{A} > 90°$ (hydrophobic), P_{ow} would be positive during drainage and negative during imbibition. A second explanation is that water hindered oil from wetting the solid surfaces during primary drainage, presumably because water initially saturated the porous medium. As water drained and the thickness of the water films decreased, oil replaced water as the wetting fluid. Subsequently, imbibing water acts as the nonwetting fluid and oil must be "forcibly" displaced from the solid surface. A third explanation for the wetting reversal could be mixed wettability of the solid. After the organosilane treatment, the sand may have both hydrophilic and hydrophobic sites, resulting in two distinct regions for the imbibition branch of the P_{ow}–S_w^{ow} curve: (i) a spontaneous imbibition region where water readily displaces oil from water-wet sites and (ii) a forced imbibition region where water "forcibly" ($P_o < P_w$) displaces oil from the oil-wet sites (7). The OTS sand displays no and the VTS sand relatively little spontaneous imbibition for water (Figure 7B). This suggests that the first two explanations are more likely; however, mixed wettability cannot be completely discounted.

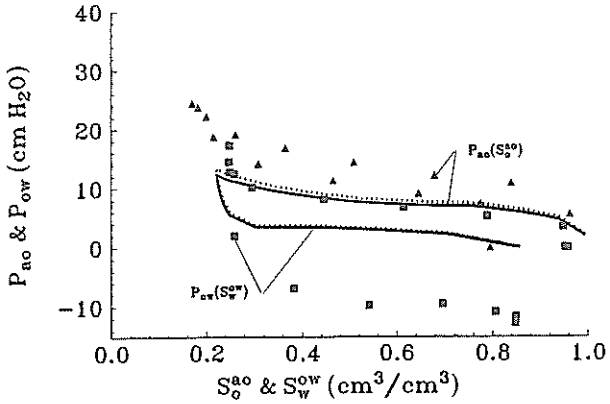

FIGURE 8. Observed and predicted P_{ao}–S_o^{ao} and P_{ow}–S_w^{ow} curves for OTS sand during drainage and imbibition. The predictions were obtained by scaling the P_{aw}–S_w^{aw} curve with σ_{ao}/σ_{aw} for P_{ao}–S_o^{ao} and σ_{ow}/σ_{aw} for P_{ow}–S_w^{ow}.

Contact Angles and Scaling. The prediction of P_c–S according to eq 4 is based on our ability to accurately measure the contact angle. The importance of reliable values for the contact angle, ϕ, is illustrated with Figure 8, which shows the actual and predicted air–oil and oil–water P_c–S curves for the OTS sand. The curves during imbibition and drainage are predicted according to eq 4, assuming $\phi_1 = \phi_2$, from the measured interfacial tensions and the P_{aw}–S_w^{aw} curve. The predicted P_{ao}–S_o^{ao} curves have a lower P_{ao} at a given S_o^{ao} than the measured P_{ao}–S_o^{ao} curves whereas the predicted P_{ow}–S_w^{ow} curves lie above the measured P_{ow}–S_w^{ow} curves. Air–oil systems will generally have lower contact angles than air–water systems because of a lower interfacial tension (in this case $\sigma_{ao} = 0.024$ N/m compared to $\sigma_{aw} = 0.072$ N/m). Ignoring differences in ϕ leads to scaled air–water data that will underestimate the P_{ao}–S_o^{ao} curve whereas scaled air–water data tend to overestimate P_{ow}–S_w^{ow} data since ϕ is greater for oil–water than air–water systems (eq 1 with $\sigma_{sa} - \sigma_{sw} > \sigma_{so} - \sigma_{sw}$). Fluids may also be contaminated, and time dependent interfacial tensions may occur (26).

The prediction of P_c–S curves can be improved by including the actual values of contact angles and by accounting for contamination. The apparent macroscopic advancing and receding contact angles (ϕ_{sld}^{A} or ϕ_{sld}^{R}) of a porous medium can be obtained by fitting a scaling parameter, β, to P_c–$\bar{S}$ curves (systems 1 and 2) during drainage and imbibition as

$$P_{c1}(\bar{S}) = \frac{\sigma_1 \cos(\phi_1^{A,R})}{\sigma_2 \cos(\phi_2^{A,R})} P_{c2}(\bar{S}) = \beta P_{c2}(\bar{S}) \qquad (8)$$

If $\phi_2^{A,R}$ is assumed to be zero, then $\cos(\phi_1^{A,R})$ can be estimated as

$$\cos(\phi_1^{A,R}) = (\sigma_2/\sigma_1)\beta \quad (9)$$

This approach is based upon the work of Morrow (*27*). The assumption that $\phi_{sao} = 0°$ for all treatments, as Figure 5 suggests, allows the use of eqs 8 and 9 to estimate ϕ_{sld}^{A} or ϕ_{sld}^{R} for other fluid pairs in the same porous medium. Hence system 1 in eqs 8 and 9 can refer to an air–water or oil–water system, while 2 refers to the air–oil system. Table 1 shows the values of ϕ_{sld}^{A} or ϕ_{sld}^{R} calculated in this manner. Values for β were obtained with the program Megafit (R. J. Lenhard, Battelle PNL, private communication), by fitting the model of van Genuchten (*28*) to two sets of P_c–S data according to the optimization procedure by Marquardt (*29*). Note that the scaling should be done between curves where the saturation for both systems is expressed in terms of either the wetting or the nonwetting fluid.

The measured value of 0.072 N/m for σ_{aw} represents pristine conditions. Use of a contaminated air–water interfacial tension, σ_{aw}^*, in scaling procedures is more realistic since even a trace amount of oil, originating from the hydrophobic tensiometers connected to the oil buret, can greatly affect σ_{aw} (*30*). The ratio, σ_1/σ_2, can also be estimated from β for systems in which $\phi_1 \approx \phi_2 \approx 0$; σ_{aw}^* was estimated as $\sigma_{aw}^* = \beta\sigma_{ao} = 0.052$ N/m from the fitted value of $\sigma_{aw}^*/\sigma_{ao}$ for the untreated sand. The estimated and measured values of σ_{aw}^* are identical. A similar value of 0.050 N/m may be obtained (cf *31*) from Antonow's relation (*32*)

$$\sigma_{aw}^* = \sigma_{ao} + \sigma_{ow} \quad (10)$$

Previous attempts to incorporate the contact angle in scaling procedures were hampered by inadequate methods for determining ϕ (*3*, *16*, *17*). Adamson (*33*) described several techniques to measure contact angles. Typically, the angle is measured, which forms after a drop of denser fluid is placed on a flat solid—a polished plate of the common mineral of the porous medium—and immersed into a less dense fluid. Silica or quartz is typically used to represent sandstone, while calcite is used if carbonates are prevalent (*34*). Contact angles measured in this manner may not accurately characterize the wetting behavior of the porous medium to due to surface roughness (*25*), immobility of adsorbed films on solid surfaces (*33*), and the different adsorptive properties of the mineral constituents (*34*). Alternatively, the aforementioned fitting procedure allows determination of an effective macroscopic contact angle. The following regression equations were derived from the results shown in Table 1 to predict contact angles for other fluid pairs

$$\phi_{sow}^{A} = 3.04\phi_{saw}^{A} - 57.64 \qquad r^2 = 0.904 \quad (11)$$

$$\phi_{sow}^{R} = 1.43\phi_{saw}^{R} + 0.39 \qquad r^2 = 0.965 \quad (12)$$

Using the fitted values for ϕ_{saw}^{A} and ϕ_{saw}^{R} from Table 1, ϕ_{sow}^{A} and ϕ_{sow}^{R} were calculated with eqs 11 and 12 to be 139.2° and 54.1°, respectively. These values compare favorably with the fitted values shown in Table 1 for the OTS treatment. The values of ϕ_{sao}^{A} and ϕ_{sao}^{R} can assumed to be zero. The P_c–S curves were calculated according to eq 4, where 2 denotes the air–water system —using $\sigma_{aw}^* =$ 0.052 N/m—and 1 can be either the air–oil or oil–water system. The measured data and the scaled curves for P_c–S of air–oil and oil–water systems are shown in Figure 9. Note that if an oil–water system is oil wet ($\phi_{sow}^{A} > 90°$ and $\beta < 0$), the P_{aw}–S_w^{aw} data are scaled to a P_{ow}–S_o^{ow} curve since both systems 1 and 2 should express the saturation in terms of the wetting fluid. The P_{ow}–S_w^{ow} curve can be obtained from the latter using $S_o^{ow} = 1 - S_o^{ow}$. Comparison of Figures 8 and 9 demonstrates that including the contact angle and the "contaminated" surface tension improves the scaling procedure.

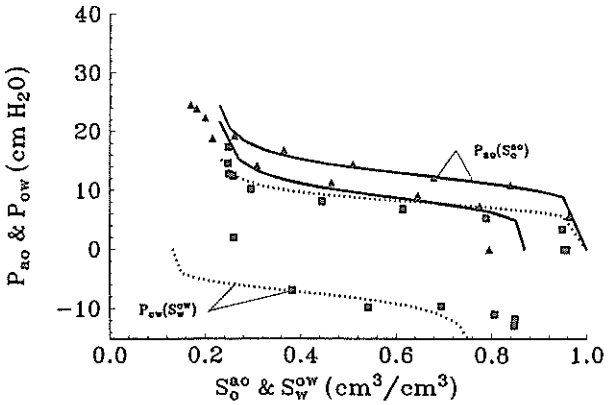

FIGURE 9. Observed and predicted P_{ao}–S_o^{ao} and P_{ow}–S_w^{ow} curves for the OTS sand during drainage and imbibition. The predictions were obtained by scaling the P_{aw}–S_w^{aw} curve according to eq 4 using measured (σ_{aw}^*, σ_{ao}, σ_{ow}, ϕ_{saw}^{A}, and ϕ_{saw}^{R}) and predicted (ϕ_{sow}^{A}, ϕ_{sow}^{R}; cf. eqs 11 and 12) values.

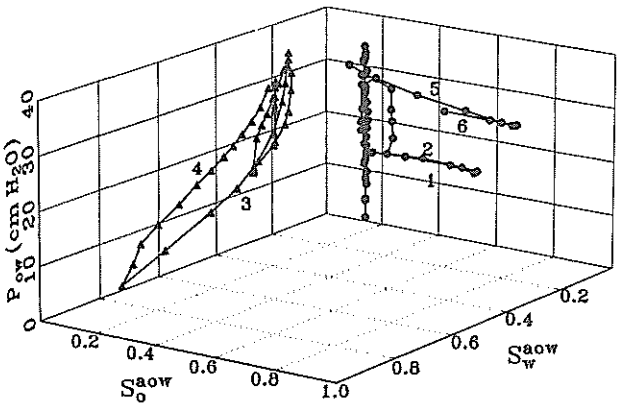

FIGURE 10. Two-dimensional projections of the measured P_{ow}–(S_w^{aow},S_o^{aow}) curve for the untreated sand, with P_{ow}–S_w^{aow} on the left side and P_{ow}–S_o^{aow} on the right side. The numbers indicate the sequence of drainage and imbibition paths: (1) imbibe oil for S_w^{aow} = 0.27; (2) drain oil for S_w^{aow} = 0.27; (3) imbibe water for S_o^{aow} = 0.14; (4) drainage water for S_o^{aow} = 0.14; (5) imbibe oil for S_w^{aow} = 0.19; (6) drain oil for S_w^{aow} = 0.19.

Three-Fluid Systems. Experimental P_c–S curves for the air–oil–water system will only be presented for untreated and OTS sands; similar results were obtained for the GPTS and VTS sands, respectively. The effect of hydrophobicity is again of particular interest.

Figure 10 shows two-dimensional projections of the $P_{ow}(S_w^{aow}, S_o^{aow})$ curve for the untreated sand, with $P_{ow}(S_w^{aow})$—for a constant oil saturation—on the left side and $P_{ow}(S_o^{aow})$—for a constant water saturation—on the right side. The values of these respective constants S_o^{aow} and S_w^{aow} are given in the caption while the numbers in the figure indicate the sequence of drainage and imbibition paths followed during the measurements. In the left vertical plane of Figure 10, P_{ow} is shown as a function of S_w^{aow} for

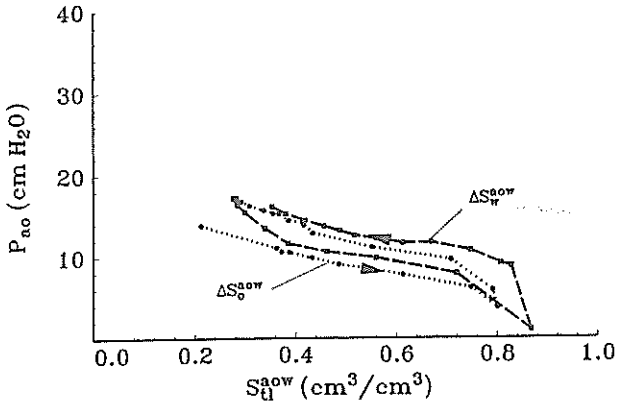

FIGURE 11. Measured P_{ao}–S_{tl}^{aow} curve for the untreated sand.

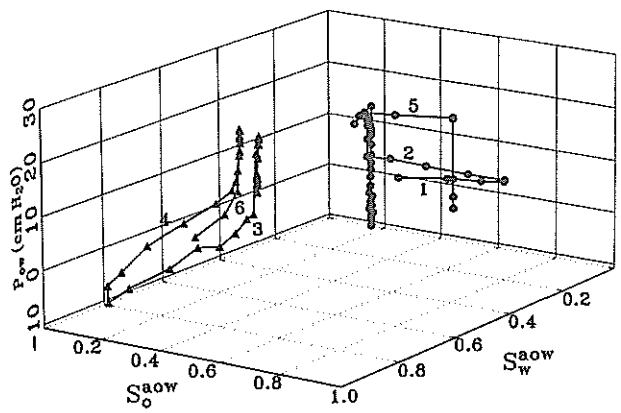

FIGURE 12. Two-dimensional projections of the measured P_{ow}–(S_w^{aow},S_o^{aow}) curve, with P_{ow}–S_w^{aow} on the left side and P_{ow}–S_o^{aow} on the right side, for the OTS (hydrophobic) sand. The numbers indicate the sequence of drainage and imbibition paths: (1) imbibe oil for S_w^{aow} = 0.27; (2) drain oil for S_w^{aow} = 0.27; (3) imbibe water for S_o^{aow} = 0.15; (4) drainage water for S_o^{aow} = 0.15; (5) imbibe oil for S_w^{aow} = 0.33; (6) imbibe water for S_o^{aow} = 0.44.

imbibition and drainage of water at a constant oil saturation of S_o^{aow} = 0.14 (curves 3 and 4). Note that P_{ow} is always positive. The right side shows P_{ow} as a function of S_o^{aow} for imbibition and drainage of oil at a constant water saturation of S_w^{aow} = 0.27 (curves 1 and 2) and S_w^{aow} = 0.19 (curves 5 and 6). The pressure drop over the oil–water meniscus mainly depends on S_w^{aow} for the untreated (hydrophilic) sand, whereas changing S_o^{aow} had little effect on P_{ow} for S_o^{aow} > 0.2.

Figure 11 shows P_{ao} as a function of S_{tl}^{aow} (=S_w^{aow} + S_o^{aow}) for the untreated sand; the P_{ao}–S_{tl}^{aow} curves are similar for both imbibition and drainage of oil and water. Leverett's assumption for water-wet conditions (eq 5) suggests that P_{ao} is completely determined by S_{tl}^{aow}, regardless of the combination of oil and water saturations. Figure 11 indicates that this is indeed the case. The scanning loops are similar to those for a two-fluid system (*35*).

Figure 12 shows results for the hydrophobic OTS sand using again the projections of the actual curves. In the left vertical plane, P_{ow} is shown as a function of S_w^{aow} for imbibition and drainage of water at S_o^{aow} = 0.15 (curves 3 and 4) and for imbibition of water at S_o^{aow} = 0.44 (curve 6). Starting with the imbibition of water, P_{ow} = P_o–P_w was negative over a large range of water contents (S_w^{aow} > 0.4). In the two-fluid oil–water system, P_{ow} was also negative for the OTS sand (Figure 7B). As oil wets the solid and displaces water for both two- and three-fluid systems, a positive pressure arises between the water relative to the

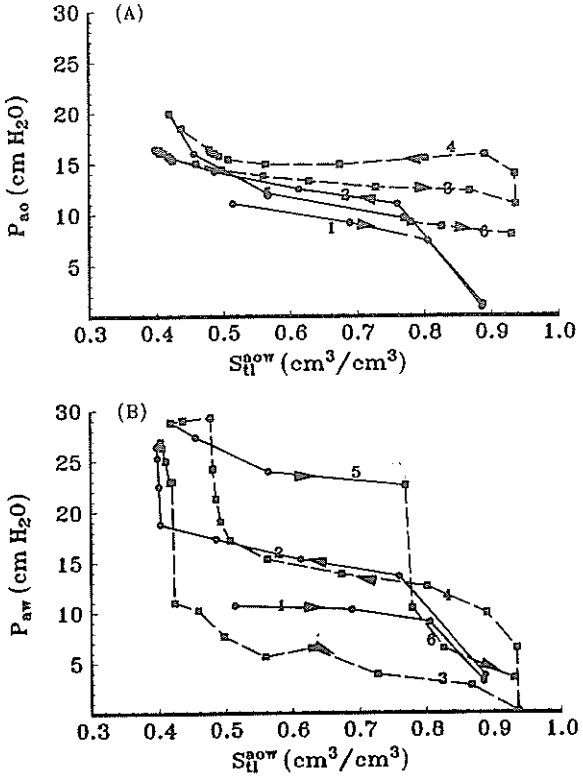

FIGURE 13. Observed (A) P_{ao}–S_{tl}^{aow} and (B) P_{aw}–S_{tl}^{aow} curves for the OTS (hydrophobic) sand. The numbers indicate the sequence of drainage and imbibition paths: (1) imbibe oil for S_w^{aow} = 0.27; (2) drain oil for S_w^{aow} = 0.27; (3) imbibe water for S_o^{aow} = 0.15; (4) drainage water for S_o^{aow} = 0.15; (5) imbibe oil for S_w^{aow} = 0.33; (6) imbibe water for S_o^{aow} = 0.44.

oil as to prevent further displacement of water by oil. The right side of the Figure 12 shows P_{ow} as a function of S_o^{aow} for imbibition and drainage of oil at S_w^{aow} = 0.27 (curves 1 and 2) and for imbibition of oil at S_w^{aow} = 0.33 (curve 5). A change in S_o^{aow} has little effect on P_{ow} (curves 1, 2, and 5) for S_w^{aow} < 0.33. If the intermediate wetting phase were continuous then eq 6 implies that P_{ow} would be a function of S_o^{aow} for oil-wet conditions; since P_{ow} is mainly a function of S_w^{aow}, it appears that the intermediate fluid is discontinuous.

Figure 13 shows both $P_{aw}(S_{tl}^{aow})$ and $P_{ao}(S_{tl}^{aow})$ for the OTS sand. If the intermediate fluid were continuous, P_{aw} should be uniquely determined by the total liquid saturation, S_{tl}^{aow}. Figure 13B shows vastly different curves and great differences in P_{aw} for the same S_{tl}^{aow}. The paths followed for imbibition and drainage of oil at S_w^{aow} = 0.27 (curves 1 and 2) and for imbibition of oil at S_w^{aow} = 0.33 (curve 5) are different from the paths followed for the imbibition and drainage of water at S_o^{aow} = 0.15 (curves 3 and 4) and for the imbibition of water at S_o^{aow} = 0.44 (curve 6). Figure 13A shows a similar behavior for $P_{ao}(S_{tl}^{aow})$. Note for that the $P_{aw}(S_{tl}^{aow})$ and $P_{ao}(S_{tl}^{aow})$ curves are different depending on whether oil (curves 1, 2, and 5) or water (3, 4, and 6) paths are followed. P_{aw} and P_{ao} are functions of both S_w^{aow} and S_o^{aow}, although they mainly depend on S_w^{aow} and S_o^{aow}, respectively. The results of Figures 12 and 13 demonstrate that hydrophobic systems, such as the OTS and VTS sands, do not behave as if they have a continuous intermediate fluid.

The above is not surprising since the coefficient for spreading of water on oil, $\Sigma_{w/o}$, is −0.074 (using σ_{aw} = 0.072 N/m) or −0.054 N/m (using σ_{aw}^* = 0.052 N/m), which

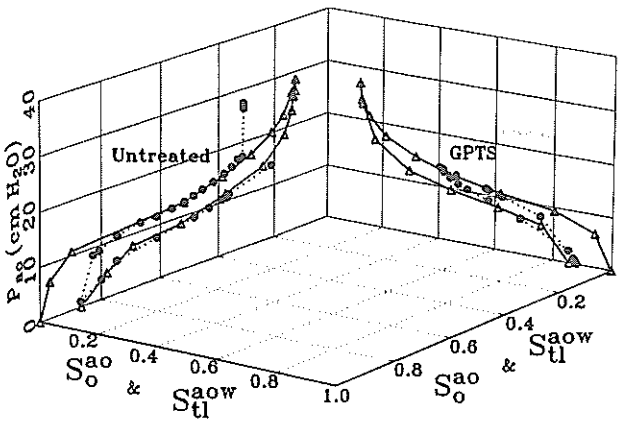

FIGURE 14. Observed two-fluid $P_{ao}-S_o^{ao}$ (△) and three-fluid $P_{ao}-S_{tl}^{aow}$ (●) curves for the untreated and GPTS sands.

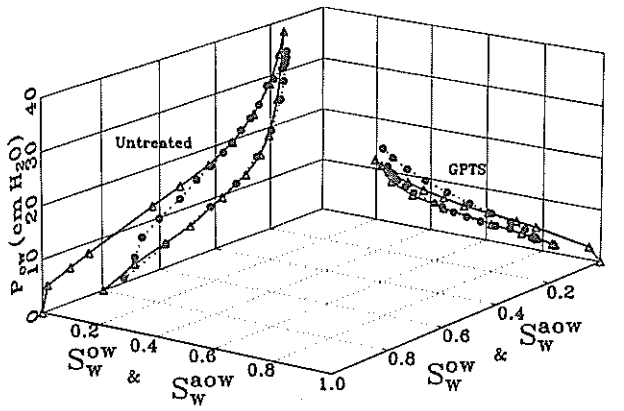

FIGURE 15. Observed two-fluid $P_{ow}-S_w^{ow}$ (△) and three-fluid $P_{ow}-S_w^{aow}$ (●) curves for the untreated and GPTS sands.

indicates that the intermediate fluid (water) does not spread between the wetting (oil) and nonwetting (air) fluids. On the other hand, in hydrophilic media oil forms a continuous intermediate layer because it spreads on water due to the value for $\Sigma_{o/w}$, i.e., 0.022 (using $\sigma_{aw} = 0.072$ N/m) or 0.002 N/m (using $\sigma_{aw}^* = 0.052$ N/m).

For the hydrophobic media there may be oil–water, air–water, and air–oil interfaces with corresponding pressures P_{ow}, P_{aw}, and P_{ao}; these are functions of both S_w^{aow} and S_o^{aow}. Changes in S_w^{aow} or S_o^{aow} are likely due to changes in air saturation; P_{aw} and P_{ao} are therefore mainly functions of S_w^{aow} and S_o^{aow}, respectively. The value for S_o^{aow} may also influence P_{aw} by limiting pores with air–water interfaces, while S_w^{aow} may similarly influence P_{ao} by restricting pores with air–oil interfaces. Figure 12 suggest that P_{ow} is virtually independent of S_o^{aow}; changes in S_o^{aow} (at constant S_w^{aow}) have apparently little effect on the oil–water interface. Conversely, water always occupies pores containing air and oil. Thus, a change in S_w^{aow} affects pores with oil–water interfaces and P_{ow} will be mainly a function of S_w^{aow}. As the system becomes saturated with liquid, P_{ow} is likely a function of S_o^{aow} because there is no air left to be displaced by oil.

Leverett's Assumption and Scaling. The experimental data for two- and three-fluid systems allow evaluation of the different scaling procedures. Figure 14 shows $P_{ao}-S_o^{ao}$ and P_{ao}-S_{tl}^{aow} curves while Figure 15 shows $P_{ow}-S_w^{ow}$ and $P_{ow}-S_w^{aow}$ curves for drainage and imbibition in untreated and GPTS sands. The two- and three-fluid P_c-S curves are very similar, suggesting that Leverett's assumption is valid for these hydrophilic media.

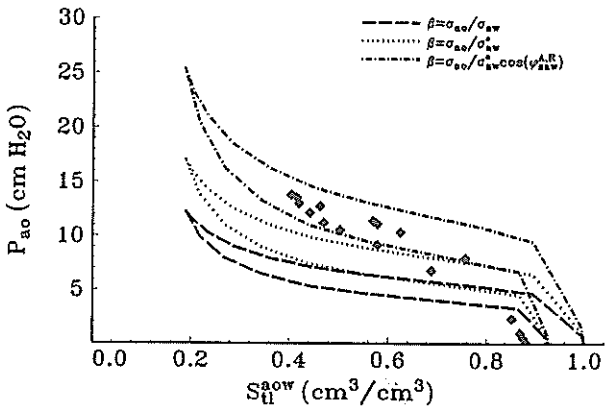

FIGURE 16. Observed $P_{ao}-S_{tl}^{aow}$ data (◆) for the GPTS sand and the $P_{ao}-S_o^{ao}$ curves predicted by scaling the $P_{aw}-S_w^{aw}$ curve using (a) σ_{ao}/σ_{aw}, (b) $\sigma_{ao}/\sigma_{aw}^*$, and (c) $\sigma_{ao}/\sigma_{aw}^* \cos(\phi_{saw}^{A,R})$.

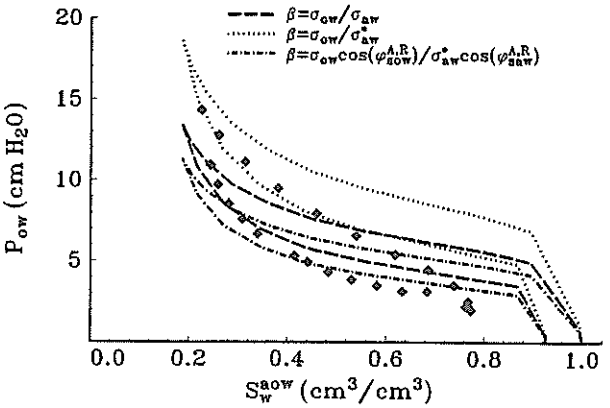

FIGURE 17. Observed $P_{ow}-S_w^{aow}$ data (◆) for the GPTS sand and the $P_{ow}-S_w^{ow}$ curves predicted by scaling the $P_{aw}-S_w^{aw}$ curve using (a) σ_{ow}/σ_{aw}, (b) $\sigma_{ow}/\sigma_{aw}^*$, and (c) $\sigma_{ow} \cos(\phi_{sow}^{A,R})/\sigma_{aw}^* \cos(\phi_{saw}^{A,R})$.

When Leverett's assumption holds, scaling three-fluid data according to eq 7 is similar to scaling two-fluid data using eq 4. Figure 16 shows observed P_{ao}-S_{tl}^{aow} data for the GPTS sand and predicted $P_{ao}-S_o^{ao}$ curves obtained by scaling actual two-fluid $P_{aw}-S_w^{aw}$ data using (a) σ_{ao}/σ_{aw}, (b) $\sigma_{ao}/\sigma_{aw}^*$, and (c) $\sigma_{ao}/\sigma_{aw}^* \cos(\phi_{saw}^{A,R})$. Note that $P_{ao}(S_o^{ao}) \equiv P_{ao}(S_{tl}^{aow})$ according to eq 5. Method c best predicts $P_{ao}(S_{tl}^{aow})$, while methods a and b underestimate P_{ao} for a given S_{tl}^{aow}. Similarly, Figure 17 shows observed $P_{ow}-S_w^{aow}$ data for the GPTS sand and predicted $P_{ow}-S_w^{ow}$ curves by scaling $P_{aw}-S_w^{aw}$ data using (a) σ_{ow}/σ_{aw}, (b) $\sigma_{ow}/\sigma_{aw}^*$, and (c) $\sigma_{ow} \cos(\phi_{sow}^{A,R})/\sigma_{aw}^* \cos(\phi_{saw}^{A,R})$. Again, note that $P_{ow}(S_w^{ow}) = P_{ow}(S_w^{aow})$ according to eq 6. Method c best predicts $P_{ow}(S_w^{aow})$; methods a and b now somewhat overestimate P_{ow}. Figures 16 and 17 demonstrate that accounting for wettability (i.e., ϕ) and contamination (i.e., σ_{aw}^*) improves the prediction of three-fluid from two-fluid data, as was already demonstrated when two-fluid curves were scaled.

The predictions of three-fluid P_c-S curves for the hydrophobic sands (OTS and VTS) using methods based upon Leverett's assumption are unreliable because of the discontinuous intermediate fluid (cf. discussion of Figure 13). Alternative methods to predict three-fluid P_c-S curves from two-fluid data need to be developed for hydrophobic systems.

Summary and Conclusions

Capillary pressure (P_c)–saturation (S) relationships in three-fluid porous media are often predicted from measured or

scaled two-fluid P_c–S curves by invoking Leverett's assumption. This procedure is based on the limiting assumptions that the porous medium is strongly wetted by one fluid and that the intermediate wetting fluid forms a continuous layer between the wetting and nonwetting fluids. To test the validity of this practice for other wetting conditions, P_c–S relations were measured for four blasting sands (three were treated with an organosilane and one was untreated) with fluid combinations (i) air and water, (ii) air and oil, (iii) oil and water, and (iv) air, oil, and water.

Two- and three-fluid P_c–S relations were obtained with an automated setup by displacing a known quantity of fluid into or from the porous medium contained in a soil column consisting of hydrophobic and hydrophilic ring tensiometers. Fluid pressures in the sample were measured with ring tensiometers connected to a pressure transducer, while fluid saturations were obtained from buret readings recorded with a pressure transducer.

The advancing and receding contact angles for the sands were quantified by curve fitting using P_c–S data from different two-fluid systems for the same porous medium. Changes in hydrophobicity had little effect on the air–oil P_{ao}–S_o^{ao} relationships, indicating that sands were strongly wetted by the oil. The contact angles for the air–water or oil–water were estimated through scaling by assuming that $\phi_{sao} = 0°$ for air–oil media. The differences in P_c–S curves for air–water and oil–water media—three treated with organosilanes and one untreated —were assumed to be due to differences in hydrophobicity and contact angle hysteresis. In hydrophobic sand systems (OTS and VTS) containing oil and water, contact angle hysteresis and the initial wetting fluid (water vs. oil) presumably caused wetting reversal in the P_c–S curves. Scaling air–water P_c–S data to predict air–oil or oil–water P_c–S curves using only the ratio of interfacial tensions should be limited to cases where the contact angles for the two systems are approximately equal. As the sands became more hydrophobic, differences in air–water, air–oil, and oil–water contact angles became pronounced and the scaled air–oil relations were underestimated ($\phi_{saw} > \phi_{sao}$), while the scaled oil–water data were overestimated ($\phi_{saw} < \phi_{sow}$). Scaling was improved by using the contaminated air–water interfacial tension and the advancing and receding contact angles.

In the hydrophilic three-fluid systems, P_{ow} and P_{ao} were observed to be unique functions of S_w^{aow} and S_{tl}^{aow}, respectively. The three-fluid P_c–S curves could be predicted from P_{ow}–S_w^{ow} and P_{ao}–S_o^{ao} curves, which may be obtained by direct measurement or scaling, as assumed by Leverett. In the hydrophobic three-fluid systems there are oil–water, air–water, and air–oil interfaces since the intermediate fluid (water) did not spread completely between the wetting (oil) and the nonwetting (air) fluids. Capillary pressures were found to depend on both S_w^{aow} and S_o^{aow}. The pressure drops P_{ow} and P_{aw} mainly depend on S_w^{aow}, while P_{ao} was chiefly a function of S_o^{aow}. We hypothesized that since a change in the saturation of one liquid is accompanied by a change in air saturation; P_{aw} and P_{ao} are mainly functions of S_w^{aow} and S_o^{aow}, respectively. The value for S_o^{aow} may also influence P_{aw} by limiting the number of pores with air–water interfaces, while S_w^{aow} may similarly influence P_{ao} by restricting pores with air–oil interfaces. The value for P_{ow} is primarily a function of S_w^{aow} since the volume of water greatly determines the oil–water interface in hydrophobic media.

The prediction of three-fluid P_c–S curves using methods based upon Leverett's assumption is less appropriate for hydrophobic media than for hydrophilic media because the intermediate wetting fluid is discontinuous. An alternative formulation for predicting these curves from two-fluid subsystems and scaling procedures needs to be developed.

Notation

a	air
d	denser fluid
GPTS	glycidoxypropyltrimethoxysilane
I	intermediate wetting fluid
l	lighter fluid
N	nonwetting fluid
o	oil
OTS	octadecyltrichlorosilane
P_c	capillary pressure (N/m^2, cm water)
P_i	pressure of fluid i (N/m^2, cm water)
P_{ij}	pressure drop over interface between fluids i and j, i.e., $P_i - P_j$ (N/m^2, cm water)
R	radius of capillary tube (m)
s	solid
S	saturation (cm^3/cm^3)
$\overline{S}$	effective saturation, i.e., $(S - S_r)/(1-S_r)$
S_i^{ij}	saturation of fluid i in a medium containing the two fluids i and j (cm^3/cm^3)
S_i^{ijk}	saturation of fluid i in a medium containing the three fluids i, j, and k (cm^3/cm^3)
S_r	residual saturation (cm^3/cm^3)
S_{tl}^{ijk}	total liquid saturation (cm^3/cm^3)
VTS	vinyltriethoxysilane
w	water
W	wetting fluid
β	scaling parameter, i.e., $\sigma_1 \cos(\phi_1^{A,R})/\sigma_2 \cos(\phi_2^{A,R})$
ϱ_b	bulk density (g/cm^3)
ϱ_o	density of oil (g/cm^3)
$\Sigma_{i/j}$	coefficient for spreading of fluid i on fluid j (N/m)
σ_{ij}	interfacial tension between fluids i and j (N/m)
σ_{aw}^*	contaminated air–water interfacial tension (N/m)
σ_k	interfacial tension of system k (N/m)
ϕ_{sij}	equilibrium contact angle at line between solid and fluids i and j
ϕ_{sij}^A	advancing contact angle
ϕ_{sij}^R	receding contact angle
ϕ_k	contact angle of system k

Literature Cited

(1) Gee, G. W.; Kincaid, C. T.; Lenhard, R. J.; Simmons, C. S. *U.S. National Report to International Union of Geodesy and Geophysics 1987–1990*; Contributions in Hydrology; American Geophysical Union: Washington, DC, 1991; pp 227–239.

(2) Hassanizadeh, S. M.; Gray, W. G. *Water Resour. Res.* **1993**, *29*, 3389–3406.

(3) Demond, A. H.; Roberts, P. V. *Water Resour. Res.* **1991**, *27*, 423–437.

(4) Leverett, M. C. *Trans. Am. Inst. Min. Metall. Pet. Eng.* **1941**, *142*, 152–169.

(5) Lenhard, R. J.; Parker, J. C. *Water Resour. Res.* **1988**, *24*, 373–380.
(6) Treiber, L. E.; Archer, D. L.; Owens, W. W. *Soc. Petr. Eng. J.* **1972**, *12*, 531.
(7) Anderson, W. G. *J. Pet. Technol.* **1987**, 1283–1299.
(8) Wilson, J. L. In *Proceeding of Conference on Fundamental Research Needs in Environmental Engineering*, Assoc. Environ. Engr. Professors: Washington, DC, 1988.
(9) Demond, A. H.; Desai, F. N.; Hayes, K. F. *Water Resour. Res.* **1994**, *30*, 333–342.
(10) Powers, S. E.; Tambin, M. E. *EOS, Trans. Am. Geophys. Union* 1993, 275.
(11) Ebsch, J. L.; Gierke, J. S. *EOS, Trans. Am. Geophys. Union* **1993**, 289.
(12) Stallard, W. M.; Choi, H. C.; Corapcioglu, M. Y.; Herbert, B. *EOS, Trans. Am. Geophys. Union* **1993**, 290.
(13) Hiemenz, P. C. *Principles of Colloid and Surface Chemistry*, 2nd ed.; Marcel Dekker Inc.: New York, **1986**; pp. 320, 345.
(14) Dullien, F. A. L. *Porous Media Fluid Transport and Pore Structure*, 2nd ed.; Academic Press Inc.: San Diego, CA 1992; p 136.
(15) Amyx, J. W.; Bass D. M.; Whiting, R. L. In *Petroleum Reservoir Engineering Physical Properties*; McGraw-Hill Book Co. Inc.: New York, 1960; p 154.
(16) Purcell, W. R. *Trans. Am. Inst. Min., Mettal., Pet. Eng.* **1949**, *186*, 39–48.
(17) Melrose, J. C. *Soc. Pet. Eng. J.* **1965**, *5*, 259–271.
(18) Lenhard, R. J.; Parker J. C. *J. Contam. Hydrol.* **1987**, *1*, 407–424.
(19) Brooks, R. H.; Corey, A. T. *Hydrology paper No.* 3, Colorado State University, Fort Collins, CO, **1965**.
(20) du Noüy, P. L. *J. Gen. Physiol.* **1919**, *1*, 521–524.
(21) *USDA–SCS Agriculture Handbook 436*; U.S. Government Printing Office, Washington, DC, 1975.
(22) Danielson, R. E.; Sutherland, P. L. In *Methods Soil Analysis, Part 1—Physical and Mineralogical Methods, 2nd ed.*; Klute, Ed.; ASA and SSSA Inc.: Madison, WI, 1986; Chapter 18.
(23) Anderson, R.; Larson, G.; Smith, C. *Silicon Compounds: Register and Review, 5th ed.*; Huls America Inc.: Piscataway, NJ, 1991.
(24) Wei, M; Bowman, R. S.; Wilson, J. L.; Morrow, N. R. *J. Colloid and Interface Sci.* **1992**, *157*, 154–159.
(25) Morrow, N. R. *J. Can. Petr. Technol.* **1975**, 42–53.
(26) Dumore, J. M.; Schols, R. S. *Soc. Pet. Eng. J.* **1974**, 437–444.
(27) Morrow, N. R. *J. Can. Pet. Technol.* **1976**, 49–69.
(28) van Genuchten, M. Th. *Soil Sci. Soc. Am. J.* **1980**, *44*, 892–898.
(29) Marquardt, D. W. *J. Soc. Ind. Appl. Math.* **1963**, *11*, 431–441.
(30) Corey, A. T. *Mechanics of Immiscible Fluids in Porous Media*; Water Resources Publications: Littleton, CO, 1986, p 20.
(31) Lenhard, R. J. *Hydrology Days*; Colorado State University: Fort Collins, CO, 1994, 223–235.
(32) Antonow, G. *J. Chim. Phys.* **1907**, *5*, 372.
(33) Adamson, A. W. *Physical Chemistry of Surfaces*, 5th ed.; John Wiley & Sons Inc.: New York, 1990; p 395.
(34) Anderson, W. G. *J. Pet. Technol.* **1986**, 1246–1261.
(35) Jury, W. A.; Gardner, W. R.; Gardner, W. H. *Soil Physics*, 5th ed.; John Wiley & Sons: New York, 1991, p 65.

Received for review June 13, 1994. Revised manuscript received February 8, 1995. Accepted March 6, 1995. [⊗]

ES9403672

[⊗] Abstract published in *Advance ACS Abstracts*, April 15, 1995.